N/Z dependence of decay channels in $A = 80$ compound nuclei

Manpreet Kaur,[1,*] BirBikram Singh,[1,†] Sarbjeet Kaur,[1] and Raj K. Gupta[2]
[1]*Department of Physics, Sri Guru Granth Sahib World University, Fatehgarh Sahib 140406, India*
[2]*Department of Physics, Panjab University, Chandigarh 160014, India*

(Received 26 July 2018; published 16 January 2019)

A comparative decay analysis of ^{80}Zr*, ^{80}Sr*, and ^{80}Kr* isobaric nuclear systems formed in ^{40}Ca + ^{40}Ca, ^{16}O + ^{64}Zn, and ^{32}S + ^{48}Ca reactions, respectively, has been conducted to investigate the N/Z dependence of different decay modes within a dynamical cluster-decay model based on the collective clusterization approach of quantum mechanical fragmentation theory. The comparative contributions of the emission of light particles (LPs), intermediate mass fragments (IMFs), and symmetric mass fragments (SMFs) in the total fusion cross-sections, σ_{fusion}, have been calculated. The results show that LPs have a major contribution to σ_{fusion} in the decay of all three compound nuclei (CN). The percentage contribution of LPs is larger for CN with higher N/Z ratio. The IMFs and SMFs cross-section are comparatively low in the total σ_{fusion} but their emissions are in competition in the decay process. The results show that the shape of mass distribution evolves from symmetric to asymmetric with increasing N/Z ratio. The yield around SMFs is greater for the system having the lowest N/Z ratio. This may be attributed to higher P_0 for the symmetric exit channel, particularly at higher ℓ values. The calculated fusion cross-sections for all three CN are in good agreement with the experimental data.

DOI: 10.1103/PhysRevC.99.014614

I. INTRODUCTION

Heavy-ion reactions are an effective probe to study the nuclear structure and the characteristics of reaction dynamics. The hot and rotating compound nuclei (CN) formed in these reactions are de-excited from the different modes ranging from the evaporation of light particles (LPs) to fission and the intermediate mass fragments (IMFs) in between these two extremes. The study of fragment production is significant due to an increased interest in the production of "exotic" nuclei via the decay of excited CN [1–3]. The formation and decay of a CN into different exit channels is significantly influenced by various degrees of freedom such as beam energy, mass of the projectile and target combination, angular momentum, projectile and target neutron-to-proton (N/Z) ratios, mass asymmetry of the projectile and target combination, etc. The entrance channel mass asymmetry (η) plays a crucial role in the determination of CN formation probability for the synthesis of superheavy elements. Studies of the heavy mass region show that η and the shell structure of the colliding partners leading to the same CN strongly affect the competition between fusion and quasifission. It has been observed that, for different mass asymmetric reactions leading to the same CN, there is an increased compound nucleus fusion probability in a mass asymmetric reaction compared to that in a symmetric mass reaction [4,5]. The different mass asymmetric reactions leading to CN with the same Z show that the shape of the mass distribution strongly depends upon the mass asymmetry [6]. Also, the study of an incomplete fusion component is reported to be influenced by mass asymmetry, which rises with increasing η [7].

Another factor that affects the reaction dynamics and the fragment production in the exit channel is the N/Z ratio of CN. Several studies have shown that the fusion process is influenced considerably by the N/Z ratios of colliding nuclei [2,8]. The study of ^{78,82}Kr + ^{40}Ca reactions shows that symmetric splitting yields are about 30% smaller for the neutron-rich system as compared to those for the neutron-deficient system [2]. The staggering in fragment cross-sections σ_A, superimposed on mass distribution, depends on the size of the emitter nuclei as well as on the N/Z ratios of the emitter nuclei. The staggering in σ_A may be due to the persistence of structure effects in fragment production mechanism. Besides, the neutron contents of emitter nuclei are apparent from the values of the IMFs cross-sections [9]. This raises the question about the N/Z dependence of different decay modes and channels, which is relatively unknown.

On the theoretical front, several approaches, such as the Hauser-Feshbach approach, the transition-state model, and the dinuclear system model [10–12], have been developed to understand the various decay modes. These models are based on distinct assumptions and involve nuclear ingredients like fission barrier and level density to study the thermal and collective properties, which influence the competition between different decay paths. The neutron-proton compositions of nuclei significantly affect these quantities [13]. Moreover, some studies near barrier have shown that the fusion mechanism is affected by the internal structures and N/Z contents of the colliding nuclei [8]. Therefore, it is important to explore the decay modes of nuclei at high angular momentum and having different N/Z ratios. Some studies have explored the role

*Current affiliation: Institute of Physics, Bhubaneswar 751005, India; manpreetphys@gmail.com
†birbikramsingh@sggswu.edu.in

 ©2019 American Physical Society

of the N/Z ratio in isotonic CN, whereas its influence in the decay of isobaric CN ranging from neutron-deficient to neutron-rich needs to be investigated further.

The influence of the discussed entrance channel parameters has been studied in the heavy mass region and needs to be further explored in the light mass region. The studies in light mass region with $40 \leqslant A_{\rm CN} \leqslant 80$ show fusion-fission process in these systems (see, e.g., Refs. [14,15] and earlier references in them). The binary decay of light mass systems with $A = 40$–80 shows a swing towards symmetric mass fission for $A = 56$–80 mass systems [14]. The CN ^{52}Fe*, ^{49}Cr*, and ^{46}V* formed in ^{12}C + ^{40}Ca, ^{9}Be + ^{40}Ca, and ^{6}Li + ^{40}Ca reactions, respectively, have been studied using coincidence technique and within the coalescence and reseparation model, which shows the symmetric splitting of these CN. Moreover, the measured energy spectra and angular distributions were found to be consistent with the decay of CN [16]. The contribution of symmetric splitting in the decay of the CN ^{70}Se* and ^{72}Sr* has been measured [17].

In the present work, we intend to investigate the decay of ^{80}Zr*, ^{80}Kr*, and ^{80}Sr* formed in ^{40}Ca + ^{40}Ca, ^{32}S + ^{48}Ca, and ^{16}O + ^{64}Zn reactions; all the CN have same excitation energy, $E^*_{\rm CN} \sim 47$ MeV, in reference to the available data [18]. Here, our aim is to address the N/Z dependence of (a) predominant LPs emissions in the decay of isobaric nuclear systems Zr*, Sr*, and Kr* having $A = 80$, and (b) the comparative contribution of IMFs and SMFs channels in the decay, within the framework of the dynamical cluster-decay model (DCM) of Gupta and collaborators [19,20].

The organization of the paper is as follows. Section II presents in brief the collective clusterization approach of the DCM. The calculations and results are discussed in Sec. III. Finally, the conclusions are given in Sec. IV.

II. THE DYNAMICAL CLUSTER-DECAY MODEL

The DCM, based on quantum mechanical fragmentation theory (QMFT) [21–23], is used to study the decay of hot and rotating CN formed in heavy-ion reactions, which is an extended version of the preformed cluster model (PCM) to study ground-state decay. The decay of excited CN is worked out in terms of (i) the collective coordinate of mass asymmetry $\eta = (A_1 - A_2)/(A_1 + A_2)$ and (ii) relative separation R, with (iii) multiple deformations β_{λ_i} (with $\lambda = 2$, 3, and 4; $i = 1$ and 2) and (iv) orientations θ_i of two nuclei in the same plane. These coordinates, η and R, respectively, characterize the nucleon division (or exchange) between outgoing fragments and the transfer of the kinetic energy of the incident channel ($E_{\rm c.m.}$) to the internal excitation [total excitation energy (TXE) or total kinetic energy (TKE)] of the outgoing channel. The TKE and the TXE of fragments are related to the excitation energy of CN as $E^*_{\rm CN} + Q_{\rm out}(T) = {\rm TKE}(T) + {\rm TXE}(T)$.

The decay cross-section of equilibrated CN, using the decoupled approximation to R and η motions, defined in terms of ℓ partial waves, is [24–26]

$$\sigma = \frac{\pi}{k^2}\sum_{\ell=0}^{\ell_{\rm max}}(2\ell+1)P_0P, \quad k = \sqrt{\frac{2\mu E_{\rm c.m.}}{\hbar^2}}, \tag{1}$$

where the preformation probability (P_0) and the penetrability (P) refer to η motion and R motion, respectively, and $\ell_{\rm max}$ is the maximum angular momentum, defined for LPs cross-section $\sigma_{\rm LPs} \to 0$, and R_a is the first turning point, defined later, where the penetration starts. The entrance channel effects in the DCM enter via the $E_{\rm c.m.}$, the maximum angular momentum $\ell_{\rm max}$, or its critical value, $\ell_{\rm crit}$, which depends on the entrance-channel mass asymmetry η [27]. The cross section for the decay of CN, denoted as the CN production cross-section or the fusion cross-section $\sigma_{\rm fusion}$, is given as

$$\sigma_{\rm fusion} = \sigma_{\rm LPs} + \sigma_{\rm IMFs} + \sigma_{\rm SMFs} + \sigma_{\rm nCN} = \sigma_{\rm CN} + \sigma_{\rm nCN}, \tag{2}$$

where $\sigma_{\rm LPs}$, $\sigma_{\rm IMFs}$, $\sigma_{\rm SMFs}$, and $\sigma_{\rm nCN}$ denote the cross sections for LPs, IMFs, SMFs, and noncompound nucleus process contribution (if any is present), respectively. In the present work, however, there is no contribution of a noncompound nucleus process. It is clear that in the DCM, the decay of the CN into LPs, IMFs, and SMFs is treated as the dynamical collective mass motion of preformed clusters or fragments through the interaction barrier.

P_0 in Eq. (1) is given by the solution of a stationary Schrödinger equation in η, at a fixed $R = R_a$:

$$\left\{-\frac{\hbar^2}{2\sqrt{B_{\eta\eta}}}\frac{\partial}{\partial\eta}\frac{1}{\sqrt{B_{\eta\eta}}}\frac{\partial}{\partial\eta} + V_R(\eta, T)\right\}\psi^\nu(\eta) = E^\nu\psi^\nu(\eta), \tag{3}$$

with $\nu = 0, 1, 2, 3, \ldots$ referring to ground-state ($\nu = 0$) and excited state solutions summed over as a Boltzmann-like function:

$$|\,\psi\,|^2 = \sum_{\nu=0}^{\infty}|\,\psi^\nu\,|^2\exp(-E^\nu/T). \tag{4}$$

Then, the probability of fragment preformation is

$$P_0(A_i) = |\,\psi(\eta(A_i))\,|^2\,\frac{2}{A_{\rm CN}}\sqrt{B_{\eta\eta}}, \tag{5}$$

where $i = 1$ or 2 and $B_{\eta\eta}$ are the smooth hydrodynamical mass parameters [28]. Evidently, P_0 assimilates the structure information of the CN which enters Eq. (3) via the fragmentation potential $V_R(\eta, T)$, which is the potential energy for all possible mass combinations A_i for each mass fragmentation coordinate η_A. The minimized fragmentation potential obtained is defined as

$$\begin{aligned} V_R(\eta, T) = &\sum_{i=1}^{2}[V_{\rm LDM}(A_i, Z_i, T)] + \sum_{i=1}^{2}[\delta U_i]\exp\left(-\frac{T^2}{T_0^2}\right) \\ &+ V_c(R, Z_i, \beta_{\lambda_i}, \theta_i, T) + V_P(R, A_i, \beta_{\lambda_i}, \theta_i, T) \\ &+ V_\ell(R, A_i, \beta_{\lambda_i}, \theta_i, T), \end{aligned} \tag{6}$$

where V_c, V_p, and V_l are the temperature-dependent Coulomb potential, the nuclear proximity potential, and the angular-momentum-dependent potential, respectively, for deformed and oriented nuclei. $B_i = V_{\rm LDM}(A_i, Z_i, T) + \delta U_i$ ($i = 1$ and 2) are the binding energies of two nuclei. $V_{\rm LDM}$ is the liquid drop energy, i.e., the macroscopic part, and δU are the "empirical" shell corrections, i.e., the microscopic part [29], of the binding energies. Temperature-dependent binding energies

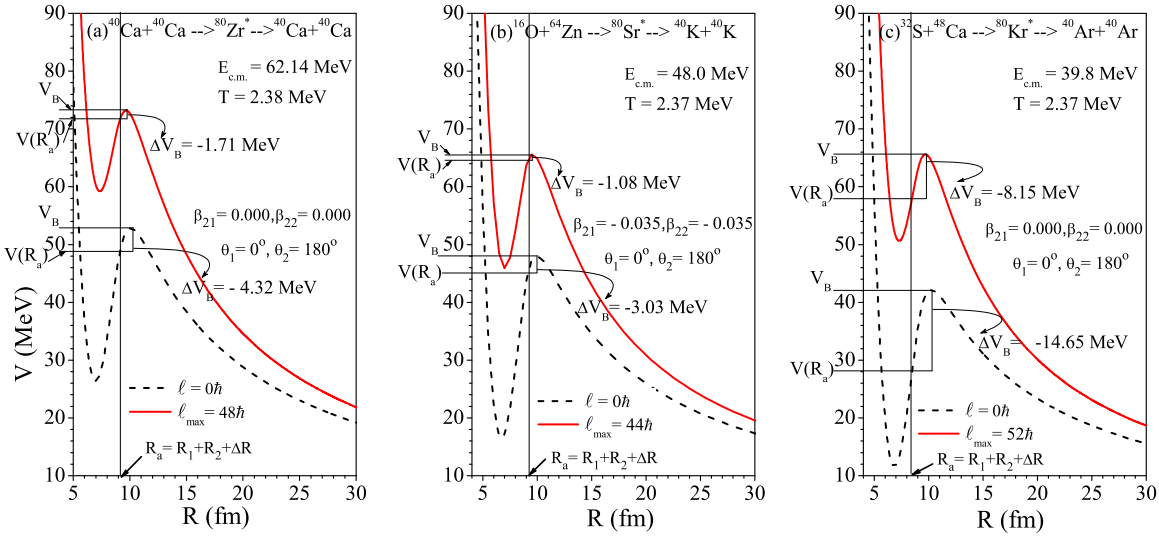

FIG. 1. Variation of scattering potential with internuclear distance R for the symmetric decay of (a) ^{80}Zr*, (b)^{80}Kr*, and (c) ^{80}Sr* with $E^*_{\rm CN} \sim 47$ MeV at $\ell = 0\hbar$ and $\ell = \ell_{\rm max}$.

were obtained from Ref. [30] with its constants at $T = 0$ refitted [24,25] to give the ground-state ($T = 0$) experimental binding energies [31], and, where the data is not available, the theoretical binding energies of Möller *et al.* [32] are used.

The penetration probability P in Eq. (1) is calculated by using the WKB integral as

$$P = \exp\left[-\frac{2}{\hbar}\int_{R_a}^{R_b}\{2\mu[V(R) - Q_{\rm eff}]\}^{1/2}dR\right], \qquad (7)$$

where $V(R)$ is the scattering potential, which is calculated as the sum of Coulomb, nuclear proximity, and angular-momentum-dependent potentials. It is solved analytically [33], with R_a as the first turning point, illustrated in Fig. 1 for the case of the respective symmetric decay of all $A = 80$ CN at $\ell = 0$ and their respective $\ell = \ell_{\rm max}$. The first turning point of the penetration path, R_a, is given as

$$R_a = R_1(\alpha_1, T) + R_2(\alpha_2, T) + \Delta R, \qquad (8)$$

with the radius vector $R_i(\alpha_i, T)$ defined as

$$R_i(\alpha_i, T) = R_{0i}(T)\left[1 + \sum_\lambda \beta_{\lambda_i} Y^{(0)}_\lambda(\alpha_i)\right], \qquad (9)$$

where

$$R_{0i}(T) = \left[1.28A_i^{1/3} - 0.76 + 0.8A_i^{-1/3}\right](1 + 0.0007T^2), \qquad (10)$$

with T calculated by using $E^*_{\rm CN} = (\frac{A}{9})T^2 - T$. The choice of parameter R_a, for a best fit to the data, allows us to relate in a simple way $V(R_a)$ to the top of the barrier V_B for each ℓ, by defining their difference ΔV_B as the effective "lowering of the barrier": $\Delta V_B = {\rm V}(R_a) - V_B$. Note that ΔV_B is defined as a negative quantity because the actually used barrier is effectively lowered, which is a built-in property of the DCM. This ensures that $V(R_a)$ ($=Q_{\rm eff}$) lies below the barrier, as illustrated in Fig. 1 for the symmetric decay of (a)^{80}Zr*, (b) ^{80}Kr*, and (c) ^{80}Sr* at $\ell = 0\hbar$ and the respective $\ell_{\rm max}$ values.

III. RESULTS AND DISCUSSION

In this section, the results for the decay of isobaric nuclear systems having $A = 80$ are presented. It is studied via the collective potential energy surface, the preformation profile, and the summed up preformation and penetration probabilities of different fragments. The contributions of LPs, IMFs, and SMFs emissions towards the total fusion cross-sections are calculated to explore the role of N/Z ratio in the reaction dynamics.

Figure 2 shows the fragmentation potential for the decay of ^{80}Zr*, ^{80}Sr*, and ^{80}Kr* at $\ell = 0\hbar$ (left panels) and $\ell = \ell_{\rm max}$ (right panels). One observes that the structure of potential energy surface changes from $\ell = 0\hbar$ to $\ell = \ell_{\rm max}$. For all the CN, LPs ($A \leqslant 4$, $Z \leqslant 2$) are energetically favorable at low angular momentum while the case is reversed at $\ell = \ell_{\rm max}$, at which the IMFs and the SMFs start competing strongly; i.e., at lower angular momenta, the LPs are energetically more favorable. The minima in the potential energy surface correspond to the stable fragments, which consequently have more preformation probabilities P_0 (Fig. 3) compared to the neighboring fragments. From Figs. 2(b), 2(d) and 2(f), it is clear that the magnitude of the potential energy minima in the fragmentation potential for ^{80}Zr* is much smaller, compared to ^{80}Kr* and ^{80}Sr* at both $\ell = 0\hbar$ and $\ell = \ell_{\rm max}$, showing that ^{80}Zr* is more fissile compared to ^{80}Sr* and ^{80}Kr*.

Furthermore, the nuclear structure effects in the decay of CN having $A = 80$, and formed at same excitation energy, $E^*_{\rm CN} \sim 47$ MeV, are analyzed through the relative preformation probability (P_0) of different fragments as shown in Fig. 3. It shows that the mass distribution changes from a U shape with minima at symmetry (at low angular momentum) [Figs. 3(a), 3(c) and 3(e)] to a bell shape with maxima around

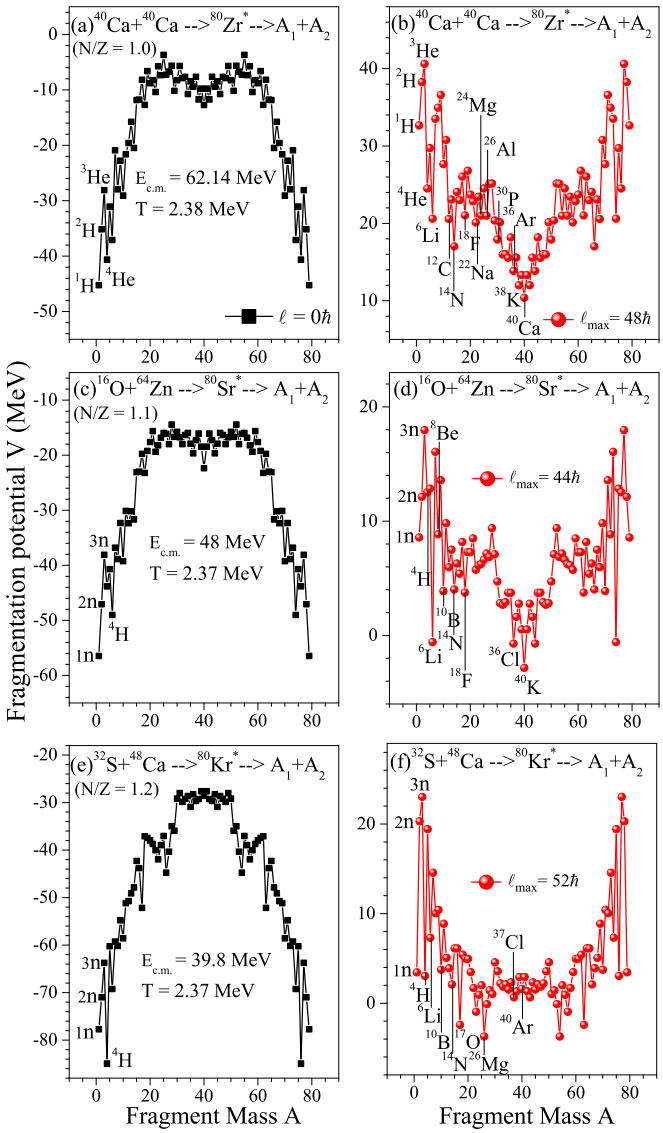

FIG. 2. Variation of the fragmentation potential V with the fragment mass A for the decay of ^{80}Zr*, ^{80}Kr*, and ^{80}Sr*, respectively, with $E^*_{CN} \sim 47$ MeV at $\ell = 0\hbar$ (left panels) and $\ell = \ell_{max}$ (right panels).

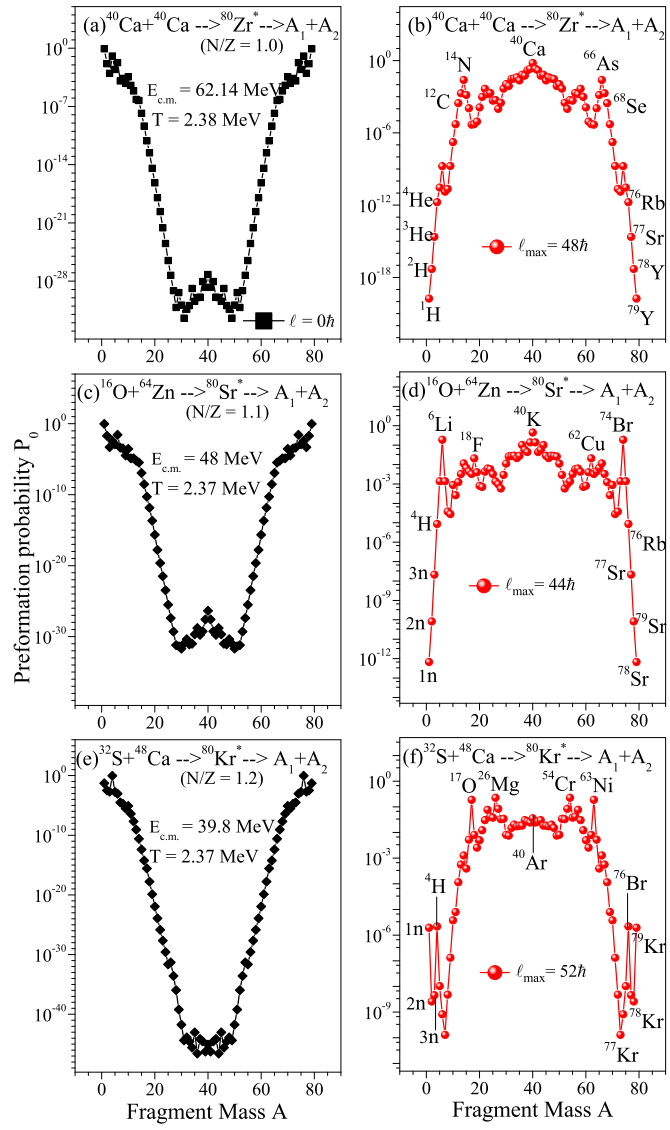

FIG. 3. Variation of the preformation probability P_0 with the fragment mass A for the decay of ^{80}Zr*, ^{80}Kr*, and ^{80}Sr*, respectively, with $E^*_{CN} \sim 47$ MeV at $\ell = 0\hbar$ (left panels) and $\ell = \ell_{max}$ (right panels).

symmetric fragments (at high angular momentum) [Figs. 3(b), 3(d) and 3(f)].

It is observed that in the decay of ^{80}Zr* [Figs. 3(a) and 3(b)], the LPs (^{1,2}H, ^{3,4}He) dominate at $\ell = 0\hbar$ but with an increase in angular momentum; i.e., for $\ell = \ell_{max}$, the SMFs ($A_{CN}/2 \pm 10$) are strongly preformed. Among the IMFs, ^{14}N has significant P_0. In the case of ^{80}Sr* [Figs. 3(c) and 3(d)], the n-rich LPs (particularly ^{4}H) are significantly preformed at both $\ell = 0\hbar$ and $\ell = \ell_{max}$.

In the decay of ^{80}Kr* [Figs. 3(e) and 3(f)], the LPs (particularly ^1n, ^{4}H) have relatively significant preformation values at both $\ell = 0\hbar$ and $\ell = \ell_{max}$. ^{26}Mg, followed by ^{17}O, is the most probable among the IMFs. It is to be noted here that maxima in the SMF window (as seen in the case of ^{80}Zr*) disappear and IMFs are in strong competition with SMFs. It is interesting to note that in Figs. 3(b), 3(d) and 3(f) the mass distribution changes from symmetric to asymmetric with increasing N/Z ratio.

To explore the role of angular momentum in the decay of CN, the variations of summed up preformation probabilities ($\sum P_0$) and summed up penetration probabilities ($\sum P$) for LPs, IMFs, and SMFs with angular momentum are shown in Figs. 4 and 5, respectively. For all three CN, in general for LPs, $\sum P_0$ is large at lower ℓ values and decreases abruptly near the ℓ_{max} value. With an increase in the ℓ value, $\sum P_0$ for IMFs shows a rise and then a fall near the ℓ_{max}, while $\sum P_0$ increases for SMFs. For ^{80}Zr* [see Fig. 4(a)], the SMFs have the highest $\sum P_0$; for ^{80}Sr* [see Fig. 4(b)], the SMFs have significant $\sum P_0$ followed by LPs and IMFs; and for ^{80}Kr* [see Fig. 4(c)], the LPs have the highest $\sum P_0$ followed by SMFs. Figure 5 shows that for ^{80}Zr* [panel (a)], the $\sum P$ values for SMFs and IMFs are more than those for LPs; for

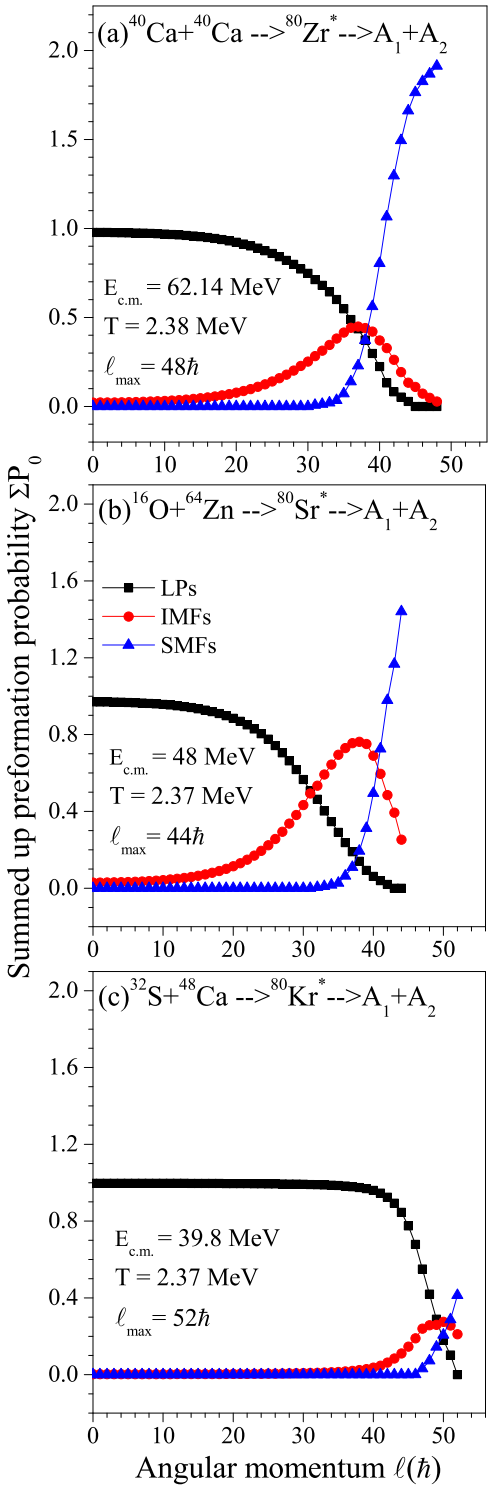

FIG. 4. Variation of the summed up preformation probability ΣP_0 with the angular momentum ℓ ($\hbar$) for the decay of (a) ^{80}Zr*, (b)^{80}Kr*, and (c) ^{80}Sr* with $E^{*}_{CN} \sim 47$ MeV.

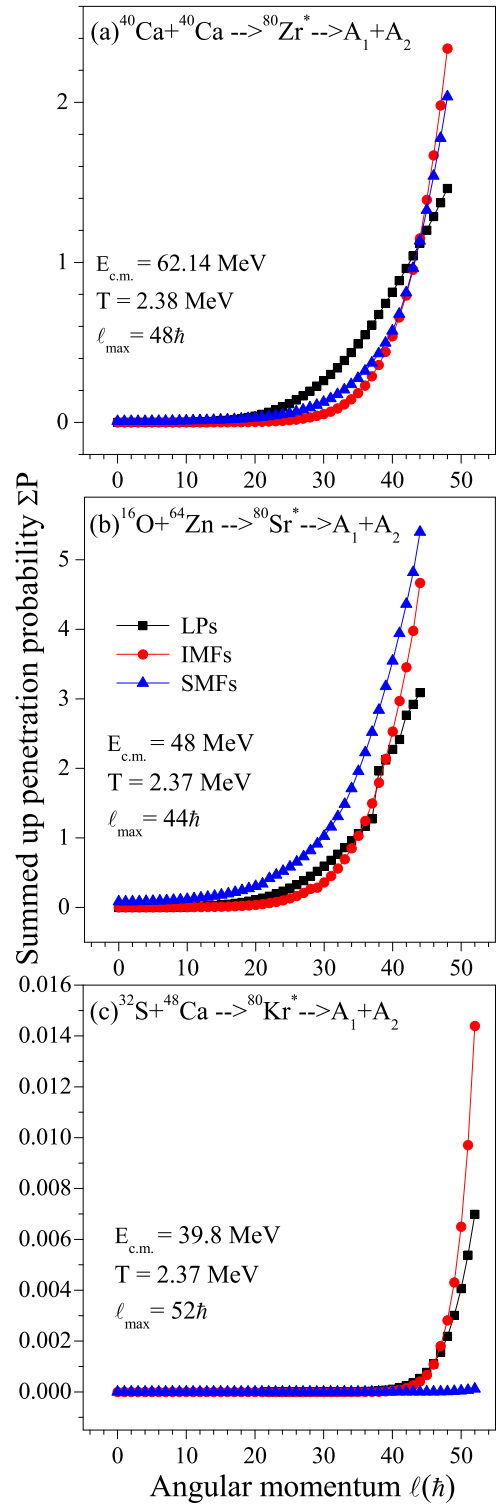

FIG. 5. Same as Fig. 4 but for the summed up penetration probability ΣP.

^{80}Sr* [panel (b)], the $\sum P$ values are the largest for SMFs followed by IMFs and LPs; and for ^{80}Kr* [panel (c)], the $\sum P$ values are the smallest for SMFs while IMFs have the highest $\sum P$ values followed by the LPs.

The above discussed factors, i.e., summed up preformation and penetration probabilities, contribute to the respective cross sections and their total sum, i.e., σ_{fusion}, which are presented in Table I. It shows comparison between the DCM calculated cross-sections for the decay of LPs, IMFs, and

TABLE I. The DCM calculated fusion cross-sections for the emissions of LPs, IMFs, and SMFs in the decay of ^{80}Zr*, ^{80}Kr*, and ^{80}Sr* formed at the same excitation energy, $E^*_{CN} \sim 47$ MeV, compared with the experimental data [18].

Reaction	N/Z ratio	$E_{c.m.}$ (MeV)	ℓ_{max} ($\hbar$)	ΔR (fm)		σ (mb)			σ_{fus}^{DCM} (mb)	σ_{fus}^{Expt} (mb)
				LPs	IMFs/SMFs	LPs	IMFs	SMFs		
$^{40}Ca + ^{40}Ca \rightarrow {}^{80}Zr^* \rightarrow A_1 + A_2$	1.0	62.14	48	1.62	1.35	373.38	20.74	50.65	444.77	438 ± 69.44
$^{16}O + ^{64}Zn \rightarrow {}^{80}Sr^* \rightarrow A_1 + A_2$	1.1	48.0	44	1.97	1.55	820.48	190.78	69.89	1081.15	1095 ± 110
$^{32}S + ^{48}Ca \rightarrow {}^{80}Kr^* \rightarrow A_1 + A_2$	1.2	39.80	52	0.72	0.72	1.35	0.013	0.0003	1.364	1.26 ± 0.26

SMFs from $A = 80$ CN. Their total sums, i.e., σ_{fusion}, have also been compared with experimental data [18], which are in good agreement. These results are further reinforced in Fig. 6, depicting the N/Z dependence of the percentage cross-section σ_x/σ_{fusion}. It follows from Table I and Fig. 6 that LPs emission is dominant in all three CN. In case of ^{80}Zr*, the SMFs contribution towards the total fusion cross-section is greater than the IMFs contribution. However, with an increase in the N/Z ratios of the CN, the percentage contribution of the SMFs cross-section decreases accompanied by an increase in the IMFs cross-section. Further, Fig. 7 shows the cross sections for different fragments, i.e., σ_A for two extreme N/Z ratio cases. An odd-even staggering of σ_A for $5 \leqslant A \leqslant 14$ fragments can be seen in the inset of Fig. 7. Moreover, it is observed that with increasing the N/Z ratio, the odd-even staggering decreases. It is to be noted that the structure in Fig. 7 follows that of the preformation profile P_0 (Fig. 3), through which nuclear structure effects in the decaying nuclear system are probed within the DCM. It indicates that staggering effects come into play due to nuclear structure effects in the fragment decay cross-sections.

IV. SUMMARY

The decay of isobaric nuclear systems ^{80}Zr*, ^{80}Sr*, and ^{80}Kr* has been studied, comparatively, within the DCM to elucidate the role of the neutron-to-proton ratio in the different decay channels. The decay products are calculated as emissions of preformed clusters with the preformation probability P_0 within the collective clusterization approach of the DCM and their subsequent penetration with the penetration probability P through the interaction potential barrier. The analysis depicts that LPs are the dominant mode of decay in all three CN and the LPs contribution towards σ_{fusion} is maximum for neutron-rich system ($N/Z = 1.2$). The IMFs and SMFs have smaller contributions in σ_{fusion} but they are competing in the decay path. The percentage contribution of SMFs is higher for the neutron-deficient system ($N/Z = 1.0$). The calculated fusion cross-sections are in good agreement with experimental data.

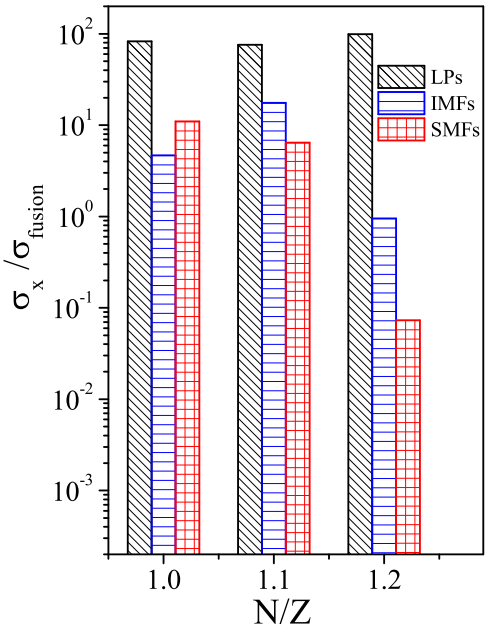

FIG. 6. Variation of the percentage cross-section σ_x/σ_{fusion} (where x symbolizes LPs, IMFs, and SMFs) with the N/Z ratio in the decay of ^{80}Zr*, ^{80}Sr*, and ^{80}Kr* having N/Z ratios of 1.0, 1.1, and 1.2, respectively.

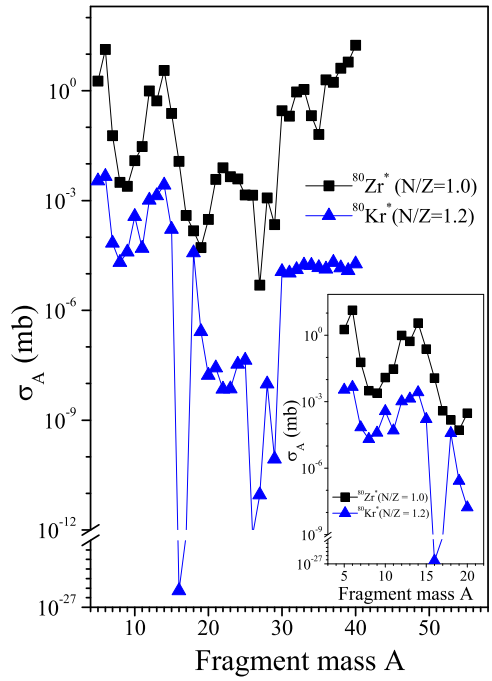

FIG. 7. Variation of σ_A with the fragment mass A in the decay of ^{80}Zr* and ^{80}Sr* nuclear systems.

[1] J. G. del Campo, C. Baktash, H. Q. Jin, D. Rudolph *et al.*, Phys. Rev. C **57**, R457 (1998).

[2] G. Ademard, J. P. Wieleczko, J. G. del Campo, M. La Commara *et al.*, Phys. Rev. C **83**, 054619 (2011).

[3] S. A. Kalandarov, G. G. Adamian, N. V. Antonenko, W. Scheid, and J. P. Wieleczko, Phys. Rev. C **84**, 064601 (2011).

[4] A. C. Berriman, D. J. Hinde, M. Dasgupta, C. R. Morton *et al.*, Nature (London) **413**, 144 (2001); D. J. Hinde *et al.*, J. Nucl. Radiochem. Sci. **3**, 31 (2002).

[5] G. Fazio, G. Giardina, G. Mandaglio, R. Ruggeri *et al.*, Phys. Rev. C **72**, 064614 (2005).

[6] P. Gippner, K. D. Schilling, W. Seidel, F. Stary *et al.*, Z. Phys. A: At. Nucl. **325**, 335 (1986).

[7] D. Singh, R. Ali, M. A. Ansari, B. S. Tomar *et al.*, Nucl. Phys. A **879**, 107 (2012).

[8] S. Pirrone, G. Politi, M. La Commara, J. P. Wieleczko *et al.*, AIP Conf. Proc. **1524**, 7 (2013); S. Pirrone, E. De Filippo, G. Politi, and P. Russotto, J. Phys.: Conf. Ser. **527**, 012030 (2014).

[9] J. Brzychczyk, D. S. Bracken, K. Kwiatkowski, K. B. Morley, E. Renshaw, and V. E. Viola, Phys. Rev. C **47**, 1553 (1993); T. S. Fan, K. X. Jing, L. Phair, K. Tso, M. McMahan, K. Hanold, G. J. Wozniak, and L. G. Moretto, Nucl. Phys. A **679**, 121 (2000).

[10] W. Hauser and H. Feshbach, Phys. Rev. **87**, 366 (1952).

[11] F. Auger, B. Berthier, A. Cunsolo, A. Foti, W. Mittig, J. M. Pascaud, E. Plagnol, J. Québert, and J. P. Wieleczko, Phys. Rev. C **35**, 190 (1987).

[12] Sh. A. Kalandarov, G. G. Adamian, N. V. Antonenko, and W. Scheid, Phys. Rev. C **82**, 044603 (2010).

[13] A. J. Sierk, Phys. Rev. Lett. **55**, 582 (1985).

[14] S. J. Sanders, Phys. Rev. C **44**, 2676 (1991); S. J. Sanders, A. Szanto de Toledo, and C. Beck, Phys. Rep. **311**, 487 (1999).

[15] C. Beck, B. Djerroud, F. Haas, R. M. Freeman *et al.*, Z. Phys. A: At. Nucl. **343**, 309 (1992).

[16] K. Grotowski, Z. Majka, R. Planeta, M. Szczodrak, Y. Chan, G. Guarino, L. G. Moretto, D. J. Morrissey, L. G. Sobotka, R. G. Stokstad, I. Tserruya, S. Wald, and G. J. Wozniak, Phys. Rev. C **30**, 1214 (1984); J. Blocki, K. Grotowski, R. Planeta, and W. J. Swiatecki, Nucl. Phys. A **445**, 367 (1995).

[17] Y. Nagame, H. Nakahara, K. Sueki, and H. Kudo, Z. Phys. A: At. Nucl. **317**, 31 (1984); J. Barrette, P. Braun-Munzinger, C. K. Gelbke, H. E. Wegner *et al.*, Nucl. Phys. A: At. Nucl. **279**, 125 (1977).

[18] P. R. S. Gomes, M. D. Rodríguez, G. V. Martí, I. Padron *et al.*, Phys. Rev. C **71**, 034608 (2005); G. Montagnoli, A. M. Stefanini, C. L. Jiang, H. Esbensen *et al.*, *ibid.* **85**, 024607 (2012); **87**, 014611 (2013).

[19] R. K. Gupta, S. K. Arun, R. Kumar, and Niyti, Int. Rev. Phys. (IREPHY) **2**, 369 (2008).

[20] R. K. Gupta, N. Singh, and M. Manhas, Phys. Rev. C **70**, 034608 (2004).

[21] J. Marhun and W. Greiner, Phys. Rev. Lett. **32**, 548 (1974).

[22] H. J. Fink, J. Marhun, W. Scheid, and W. Greiner, Z. Phys. **268**, 321 (1974).

[23] R. K. Gupta, W. Scheid, and W. Greiner, Phys. Rev. Lett. **35**, 353 (1975).

[24] R. K. Gupta, R. Kumar, N. K. Dhiman, M. Balasubramaniam, W. Scheid, and C. Beck, Phys. Rev. C **68**, 014610 (2003).

[25] B. B. Singh, M. K. Sharma, and R. K. Gupta, Phys. Rev. C **77**, 054613 (2008).

[26] B. B. Singh, M. Kaur, V. Kaur, and R. K. Gupta, EPJ Web Conf. **86**, 00048 (2015); JPS Conf. Proc. **6**, 030001 (2015); M. Kaur, B. B. Singh, S. K. Patra, and R. K. Gupta, Phys. Rev. C **95**, 014611 (2017).

[27] B. B. Singh, M. K. Sharma, R. K. Gupta, and W. Greiner, Int. J. Mod. Phys. E **15**, 699 (2006).

[28] H. Kröger and W. Scheid, J. Phys. G: Nucl. Phys. **6**, L85 (1980).

[29] W. D. Myers and W. D. Swiatecki, Nucl. Phys. A **81**, 1 (1966).

[30] N. J. Davidson, S. S. Hsiao, J. Markram, H. G. Miller, and Y. Tzeng, Nucl. Phys. A **570**, 61 (1994).

[31] G. Audi and A. H. Wapstra, Nucl. Phys. A **595**, 409 (1995); G. Audi, A. H. Wapstra, and C. Thiboult, *ibid.* **729**, 337 (2003).

[32] P. Möller, J. R. Nix, W. D. Myers, and W. J. Swiatecki, At. Data Nucl. Data Tables **59**, 185 (1995).

[33] S. S. Malik and R. K. Gupta, Phys. Rev. C **39**, 1992 (1989).